Dayside Electrodynamics Observed by Polar with Northward IMF

N. C. Maynard[1], W. J. Burke[2], D. R. Weimer[1], F. S. Mozer[3], J. D. Scudder[4], C. T. Russell[5], and W. K. Peterson[6]

We present measurements of electric/magnetic fields and energetic particle fluxes acquired during two Polar passes above the northern dayside ionosphere. The WIND satellite determined that in both instances the interplanetary magnetic field (IMF) had northward components, similar clock angles in the Y_{GSM} - Z_{GSM} plane, and comparable intensities. At different times during the passes Polar encountered particle fluxes with central plasma sheet (CPS), boundary layer, cusp and polar cap spectral characteristics. Electric fields measured during cusp/boundary layer passages are marked by very large variability with variations extending from the PC 1 through the PC 4 ranges. Although the orbital paths of Polar during the two passes followed similar trajectories, the large-scale dynamics encountered were different. In one instance the downward moving ions displayed a "reverse", velocity-dispersion feature, with the highest energies detected near the poleward boundary of the cusp, indicating that Polar crossed magnetic field lines that map upward to a merging region poleward of the cusp. The cusp was part of a counter-clockwise rotating (positive potential) cell, adjacent to a negative potential afternoon cell, which included precipitation from CPS and boundary layer sources. In the other case, Polar exited a wide boundary layer directly into the polar cap, where it detected a clockwise-rotating (negative potential) lobe cell, poleward of its merging line. We compare electric potential distributions detected at altitudes near 5 R_E with observations from satellites in low-Earth orbit and predictions of a model derived from them, under prevailing solar wind conditions.

[1] Mission Research Corporation, Nashua, New Hampshire
[2] Phillips Laboratory, Hanscom Air Force Base, Massachusetts
[3] Space Sciences Laboratory, University of California, Berkeley
[4] Department of Physics and Astronomy, University of Iowa, Iowa City
[5] Institute for Geophysics and Planetary Physics, University of California, Los Angeles
[6] Lockheed Martin Space Sciences Laboratory, Palo Alto, California

Geospace Mass and Energy Flow: Results From the International Solar-Terrestrial Physics Program
Geophysical Monograph 104

INTRODUCTION

The entry of particles and electric fields from the interplanetary medium into the Earth's magnetosphere during periods of northward IMF has been studied using a broad spectrum of ground- and space-based sensors. The dayside magnetosphere quickly responds to changes in the polarities of IMF B_Y and/or B_Z. Within a few minutes (approximately an Alfvén travel time) of the changes reaching the magnetopause, characteristic optical [*Sandholt*, 1991; *Sandholt et al.*, 1996; *Murphree et al.*, 1990] and plasma convection signatures [*Clauer and Friis-Christensen*, 1988] appear in the ionospheric projection of the cusp. The changes are believed to result from a shift in

the site of magnetic merging between the IMF and the Earth's field from equatorward of the cusp with IMF $B_Z <$ 0 to the poleward boundary of the cusp with $B_Z > 0$ [*Russell*, 1972].

If the IMF retains a northward orientation for longer than a half hour significant changes appear in global ionospheric convection patterns. *Maezawa* [1976] reported detecting magnetic perturbations during the Antarctic summer, indicating that regions of sunward convection develop in the polar cap when the IMF is northward. Electric and magnetic fields measured by the S3-2 [*Burke et al.*, 1979], Atmospheric Explorer [*Reiff and Heelis*, 1994] and MAGSAT [*Iijima and Shibaji*, 1984] satellites suggested that with IMF $B_Z > 0$ and $B_Y \sim 0$, a four-cell convection patterns evolves. The pattern consists of two cells in the central polar cap, which are of opposite polarity to the standard negative afternoon cell and positive morning cell and are driven by merging at the poleward boundary of the cusp [*Dungey*, 1961; *Russell*, 1972], and a weak but standard-polarity pair of cells in the auroral oval, possibly driven by the low latitude boundary layer [*Eastman et al.*, 1976]. Using electric field measurements of the DE 2 satellite, *Heppner and Maynard* [1987] showed that during periods of northward IMF in which B_Y has large values, two distorted convection cells operate at high latitudes. The sense of cell rotation is the same as that observed with IMF $B_Z < 0$, but the axis of symmetry for the two cells is rotated far from the noon-midnight meridian. The orbits used by *Heppner and Maynard* [1987] to infer the convection pattern with $B_Z > 0$ and $B_Y > 0$ were reexamined by *Burke et al.* [1994] using simultaneous measurements from the retarding potential analyzer [*Hanson et al.*, 1981] and electron spectrometer [*Winningham et al.*, 1981] on DE 2. These provided supplementary information about the directions of convection flow lines (equipotentials) crossing the selected DE 2 trajectories and about the source regions of precipitating electrons. They concluded that the afternoon (negative potential) cell is rotated into the prenoon sector and consists of two parts: (1) equipotentials whose associated magnetic flux is always open, and (2) equipotentials whose associated flux is both open and closed. Equipotentials with circulating open flux, hereafter referred to as lobe cells [*Reiff and Burch*, 1985], are embedded within the afternoon cell and have the same sense of rotation.

Passages of satellites through the dayside high-latitude ionosphere are marked by encounters with distinctive particle and field characteristics. *Newell et al.* [1991a, b] have identified the spectral properties of electrons and ions in the dayside ionosphere whose magnetospheric sources are the central plasma sheet (CPS), the low-latitude boundary layer (LLBL), the cusp and the mantle. In energy-versus-time spectrograms the cusp is marked by intense fluxes of low energy (<100 eV) electrons and energy-dispersed ions. The latter signature is a time-of-flight, velocity-filter effect. During periods of northward (southward) IMF, the highest energy ions are detected near the poleward (equatorward) boundary of cusp precipitation [*Reiff et al.*, 1980; *Burch et al.*, 1980]. *Maynard* [1985] showed that cusp entry is also marked by a significant increase in the level of low-frequency noise measured by electric field sensors. The rapid traversal of the cusp by satellites in low-altitude orbits only allows for the detection of waves in the Pc-1 band [*Maynard*, 1985; *Basinska et al.*, 1992]. Satellite crossings of the ionospheric projections of magnetopause merging sites are frequently marked by electromagnetic spikes at the equatorward [*Maynard et al.*, 1991] and poleward [*Basinska et al.*, 1992] boundaries of cusp precipitation during periods of southward and northward IMF, respectively. On larger scales, ionospheric plasma convection in the cusp has a sunward (poleward) component when the IMF has a northward (southward) component. The azimuthal component of convection is controlled by the polarity of IMF B_Y. Convection is westward in the northern hemispheric cusp when IMF $B_Y > 0$. The opposite polarity relationship maintains in the southern hemisphere cusp. Finally we note that besides the large scale, Region 1/Region 2 systems, the dayside ionosphere is marked by cusp and mantle field-aligned current (FAC) systems, often referred to as Region 0 [*Iijima and Potemra*, 1976; *Erlandson et al.*, 1988].

Empirical models for patterns of high-latitude potentials (convection) have been constructed for various solar wind/IMF conditions. These have been based on pattern recognition normalization technique using the DE-2 data set [*Heppner and Maynard*, 1987] and average values from the large DMSP data bases [*Rich and Hairston*, 1994]. Recently *Weimer* [1995, 1996] has developed a technique that uses least-squares fits of spherical harmonics that also includes effects of the dipole tilt angle. Published representations of the modeled convection patterns appear to be quite complex, especially for periods with IMF $B_Z >$ 0 and $|B_Y| \leq B_Z$. Multiple small cells evolve within larger convection cells.

This paper presents electric/magnetic field and particle measurements acquired by instrumentation on the Polar satellite during two passes at dayside, high latitudes in extended periods of northward IMF in which $|B_Y| \leq B_Z$. The following section contains brief descriptions of Polar sensors used in this study. The observations section

describes particle and field measurements taken at middle altitudes by Polar on April 3, and 8, 1996. Interpretations of the observations in terms of Polar encounters with middle altitude projections of previously identified magnetospheric plasma regimes are presented in the final section. We also compare Polar measurements of high-latitude convection with the predictions of the *Weimer* [1995, 1996] model under prevailing interplanetary conditions.

INSTRUMENTATION

Polar was launched into a 90° inclination orbit from the Western Test Range at Vandenburg, California on February 24, 1996. The initial orbital plane was in the early post-noon/midnight local time sectors. Apogee (above the northern polar cap) and perigee are at geocentric distances of 9 and 1.8 R_E, respectively. The spacecraft is spin stabilized at 10 rpm, with its spin axis perpendicular to the orbital plane. The three instruments whose measurements are used in this study are the electric field instrument (EFI), the magnetic field investigation (MFI), and the HYDRA electron/ion spectrometer. Comprehensive descriptions of these sensors are provided by *Harvey et al.* [1994], *Russell et al.* [1994], and *Scudder et al.* [1994], respectively. Only brief summaries of their relevant capabilities are provided below.

EFI consists of three dipoles to measure vector electric fields from potential differences between three pairs of spherical sensors. Two of the pairs of sensors are held at separation distances of 100 m and 130 m by wire booms that move in the spacecraft's spin plane. The third pair is held at a separation of 14 m by a pair of rigid booms, aligned with the spin axis. The two spin-plane components of the electric field are represented by the symbols E_{X-Y} and E_Z. E_{X-Y} is the projection of the spin-plane component of the electric field onto the GSE (geocentric solar ecliptic) plane. It is positive whenever the unit vector has a component in the $-X_{GSE}$ direction. E_Z is positive toward the GSE north pole. The third component, E_{56}, points along the spin axis, positive in the sense that completes an orthogonal, right-hand coordinate system. Thus with Polar orbiting in the noon meridian, components of the vector (E_{X-Y}, E_Z, E_{56}) are positive in the ($-X_{GSE}$, $+Z_{GSE}$, $+Y_{GSE}$) directions. Data are sampled at a rate of 40 s^{-1} by all three sensors. Corrections must be made for dc offsets and fields induced by satellite's motion ($-\mathbf{V_s} \times \mathbf{B}$) and by transformation of the measurements into the corotating frame. In addition, to eliminate magnetic wake effects at lower densities, data taken when a sensor axis was within an avoidance angle to the magnetic field were eliminated. The remaining data have been fit to a sine wave. The optimum avoidance angle value varies with density and is given for each data set below. Spin-fit measurements are presented below every 6 s for E_{X-Y} and E_Z. Measurements of E_{56} by the short booms are contaminated by unknown levels of dc offsets. To estimate their values we normally make independent calculations of E_{56} using the $\mathbf{E} \cdot \mathbf{B} = 0$ condition. However, in the two cases chosen for analysis, the magnetic field vector lay very close the spin plane. This extrapolation then causes small uncertainties in the spin plane to be multiplied by large factors which creates large uncertainties in the extrapolated E_{56} value. For this reason we present in this paper only the electric field's spin-plane components.

MFI consists of two orthogonal, triaxial fluxgate magnetometers that are mounted on a nonconducting boom at separation distances from the nearest satellite surface of 5.97 m and 4.75 m. the outer sensor operates in two ranges ±5525 nT and ±694 nT; the inner sensor in the ranges ±46,700 nT and ±5860 nT. Data are sampled at a rate of 500 s^{-1} in all three components and averaged with a recursive filter to provide data at 100 samples per second and 8 samples per second. Only 8 samples per second data are available for the times under study here. In this study we are mostly concerned with magnetic perturbations produced by currents that couple the high-latitude to the magnetosphere or magnetosheath along closed or open magnetic field lines, respectively. Since these large-scale FAC systems generally extend much further in longitude than latitude [*Iijima and Potemra*, 1976], associated magnetic perturbations are mostly in the azimuthal component B_{56}. Positive-slope deflections in B_{56} with time (latitude) are detected as the northward-moving Polar crosses FAC sheets directed into the ionosphere.

The HYDRA instrument consists of two pairs of electron and ion/electron spectrometers, each mounted 180° apart on the spacecraft body. In this paper we only use ion and electron measurements from the Duo Deca Electron Ion Spectrometer (DDEIS). As the name suggests, DDEIS is made up of six pairs of 127° electrostatic analyzers looking in different directions outward on a unit sphere. Each measures the fluxes of ions and electrons in 55 energy steps between 10 eV/q to 10 keV/q with a resolution in energy of $\Delta E/E = 6\%$, and angle of 10°. Fully three-dimension distribution functions for electrons and ions are acquired in 0.5 s.

OBSERVATIONS

This section presents particles and fields measured by Polar during dayside passes on April 3, and April 8, 1996.

Table 1. Interplanetary conditions

Date	SW Speed	B_X	B_Y	B_Z
4/3/96	353 km/s	-0.3 ±0.5 nT	3.1 ±0.8 nT	5.1 ±1.0 nT
4/8/96	312 km/s	0.9 ±0.8 nT	6.4 ±0.5 nT	7.0 ±0.4 nT

In both cases the satellite was moving toward higher altitudes and northern-hemisphere latitudes. Average solar wind speeds (km/s) and the interplanetary magnetic field (nT) X_{GSM}, Y_{GSM} and Z_{GSM} components along with the variability over 40 min are summarized for the periods of interest in Table 1. The data come from the WIND satellite located near (X_{GSM}, Y_{GSM}, Z_{GSM}) of (76.9, 2.1, 0.3) R_E and (82.1, 27.5, -2.8) R_E on April 3, and April 8, respectively. Since interplanetary conditions were stable across the studied interval, and we are primarily interested in steady-state responses of the magnetosphere, knowing exact propagation times between WIND and the Earth are not critical for this study. Table 1 shows that in both cases the solar wind speed was in the low-to-moderate range. The IMF had substantial, positive Y_{GSM} and Z_{GSM} components, with $B_Y < B_Z$, and with $B_X \sim 0$. on April 3. It had comparable values on April 8. We note that the level of geomagnetic activity was low on both days, during the times of interest, with K_P indices of 2- and 2, respectively.

The remainder of this section is divided into two parts which present Polar observations first from April 8, then April 3. Here our task is to present physical quantities measured by the three sensors and point out empirical relationships between them. Interpretations, especially of potentially controversial aspects, are relegated to the discussion section. Because of their greater familiarity for identifying source regions, we show HYDRA measurements before those from EFI/MFI.

April 8, 1996

Plate 1A displays electron (top) and ion (bottom) differential energy flux accumulated in 24 ms intervals by DDEIS from 1400 to 1700 UT on April 8, 1996, in an energy-versus-time spectrogram format. Averages over 13.8 s of data acquisition of these fluxes per 24 ms values are displayed, with each spectra representing the average over 72 such readings of the fluxes at the indicated energy. The color bar indicates flux intensities. The dashed lines crossing the two spectrograms represent the time dependence of the average energies of the sampled populations. The measurements are presented as functions of universal time (UT), invariant latitude (ILT), magnetic local time (MLT) and geocentric distance in R_E. Values of the ILT, determined using IGRF 95, are related to the magnetic L shell by the familiar relationship

$$ILT = \cos^{-1}(1/L^{-1/2})$$

On a purely empirical basis, the particle measurements from April 8 divide into four time intervals. (1) Prior to 1500 UT the highest ion count rates were at energies in the 8 to 3 keV/q range. The energy of peak flux decreased with increasing ILT. Electron fluxes were high (>100) at energies below 60 eV and low (<10) at energies above 100 eV. Their sharp spectral cutoff suggests that low-energy population mostly consists of atmospheric photoelectrons [*Doering et al.*, 1976]. (2) The period between 1500 and 1505 UT is marked by a burst of electrons with energies between 200 eV and 2 keV. A similar increase in the flux of ions with ~5 keV/q was detected simultaneously. (3) The third period extends from 1505 to 1540 UT and is marked by nearly constant fluxes of electrons with energies <200 eV and dynamic variations in the ion measurements. From about 1505 to 1515 UT the energies of highest ion fluxes decreased from 4 to 0.2 keV/q. With notable small-scale variations, average ion energies remained within 0.2 - 0.3 keV/q until 1526 UT when they began to increase systematically to 2 keV/q at 1537 UT. Phenomenologically, we describe the changing ion spectral characteristics at 1501 - 1508 UT and 1526 - 1537 UT as "standard" and "inverse" ion dispersion events. (4) After 1540 UT, DDEIS detected electron fluxes whose intensities and energies were significantly reduced, and ion count rates near background levels. Based on experience with the spectral characteristics of ion and electron fluxes observed at low altitudes [*Newell et al.*, 1991a, b], we identify the source regions encountered by Polar during the first interval as the central plasma sheet (before 1500 UT), and during the fourth interval as the polar cap (after 1540 UT), respectively. Interpretation of the source regions for particles observed during the second and third segments is deferred.

Figure 1 shows the spin-plane components of the electric field, the electric potential distribution along Polar's trajectory, and the spin-axis components of the plasma drift V_{56} and magnetic field B_{56} with the T96 model field [*Tsyganenko*, 1996] subtracted. A magnetic

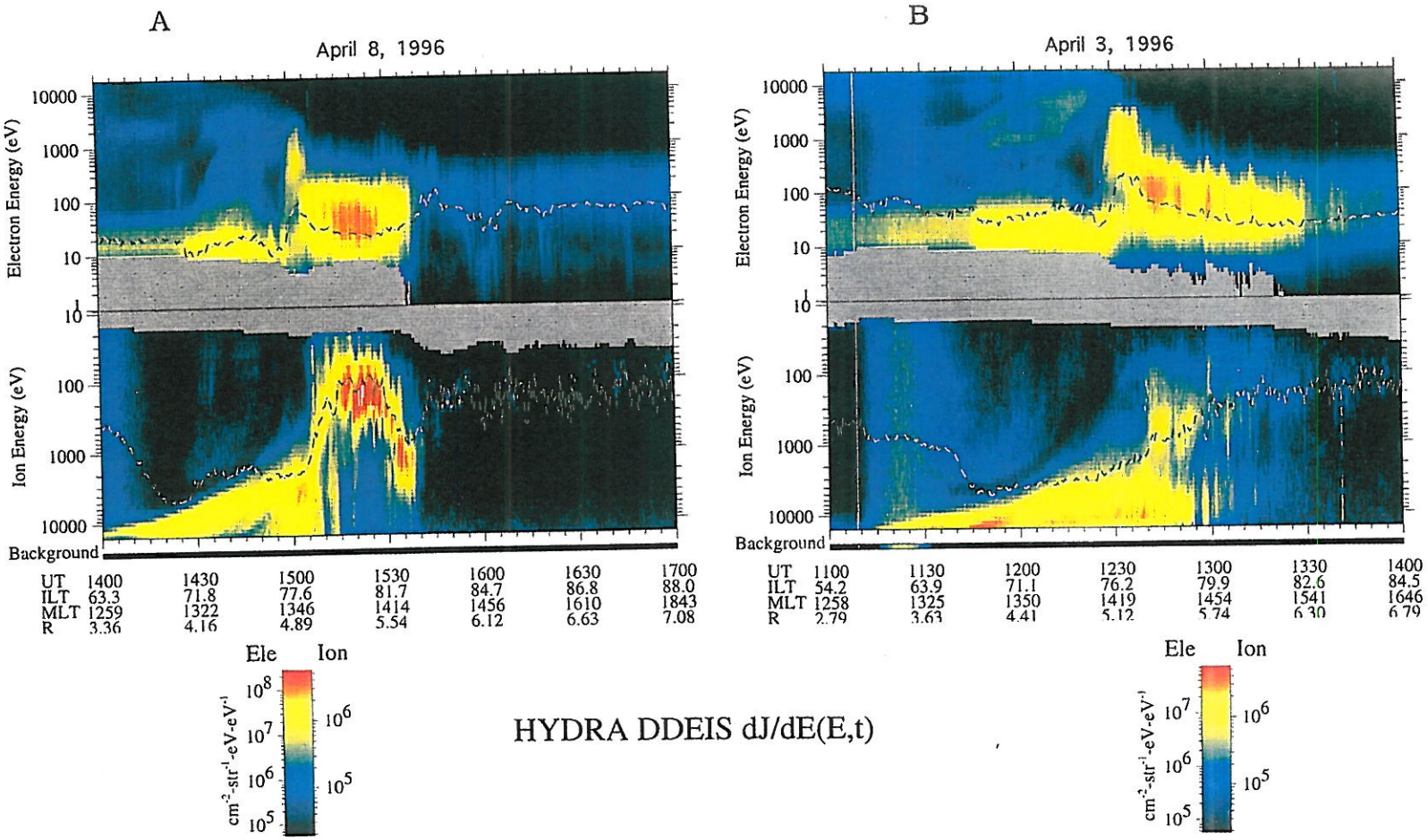

Plate 1. Energy-versus time spectrogram showing differential energy flux detected by HYDRA of electrons (top) and ions (bottom) with energies between 10 eV/q and 20 keV/q from (A) 1400 – 1700 UT on April 8, 1996 and from (B) 1100 – 1400 UT on April 3, 1996 (see text). The lowest energies are displayed at the center of the spectrogram. The measured energies have been adjusted in accordance with the spacecraft potential determined by the electric field instrument (gray areas at the top of the ion spectrogram and the bottom of the electron spectrogram). Color bars are different and are given under each spectrogram.

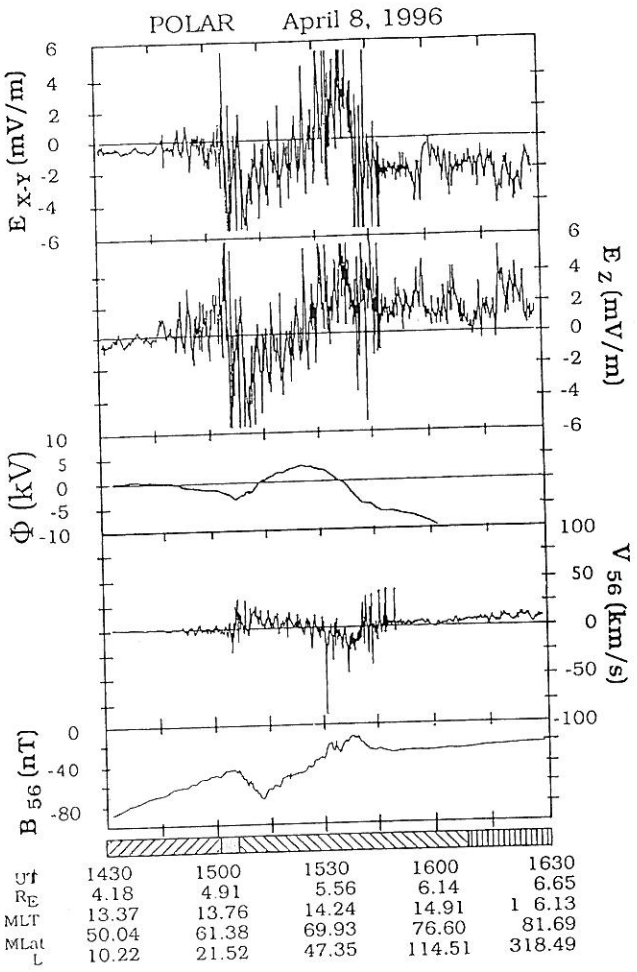

Figure 1. Electric and magnetic field measurements from 1430 – 1630 UT on April 8, 1996. From top to bottom the panels give the electric field spin-plane components $E_{X\text{-}Y}$ and E_Z, the electric potential ϕ derived from an integration along the Polar trajectory, the plasma-drift V_{56} and magnetic field B_{56} component transverse to the orbital plane. We have subtracted the *Tsyganenko* [1996] T96 model field from the B_{56} measurement to obtain the values plotted. Data are displayed as functions of universal time, the geocentric distance of the satellite, magnetic local time, magnetic latitude and L shell. The four particle regions described in the text are marked at the bottom of the figure for reference}

field avoidance angle of 0° up through 1550 UT and 45° thereafter was used for the electric field spin fits. Potential values are for the corotating reference frame for easy comparison to the ionospheric patterns. Since the satellite velocity $\mathbf{V_S}$ lies very close to the spin plane, estimates of the potential distribution along the trajectory

$$\phi = \int -\mathbf{E} \bullet \mathbf{V_S}\, dx$$

should be accurate, despite our lack of knowledge about E_{56}. Its utility for understanding geomagnetic processes requires that the convection pattern be relatively steady over the interval in which the measurements were acquired. The steady conditions observed by WIND in the interplanetary medium provides justification for this an assumption. Likewise our calculation of the V_{56} component of

$$\mathbf{V} = (\mathbf{E} \times \mathbf{B})/|B|^2$$

requires no knowledge of E_{56}. For reference, we have marked the four different particle-flux segments at the bottom of the figure.

Attention is directed to the following seven points. (1) Prior to 1452 UT, the absolute values and variability of electric field was <1 mV/m. After this the amplitudes of variations grew. (2) From 1503 to 1542 UT the amplitude of electric field variations assumed values <5 mV/m. The periods of the variations ranged from a few tens of seconds to a few minutes (Pc 1 to Pc 4). (3) Average (quasi dc) values of the $E_{X\text{-}Y}$ and E_Z show similar variations, with the polarity of both components reversing near 1525 UT. (4) The third panel shows Polar crossed two regions of negative potential that bound a region of positive potential (1512 - 1534 UT). Viewed from above the north pole, the sense of rotation for plasma convection is clockwise/counterclockwise in regions of negative/positive potential (for instance, see patterns of *Heppner and Maynard* [1987]). In this case the potential of the counterclockwise rotating cell is ~3 kV. (5) The east-west component V_{56} had low values prior to 1504 UT. From 1504 to 1526 UT Polar detected eastward flow (positive V_{56}), with an average value of ~10 km/s, as it crossed the region of "standard" ion dispersion and of low-energy, ion/electron fluxes. An average westward flow (negative V_{56}) of ~10 km/s to the west marked the "inverse" dispersion event. This is consistent with counterclockwise plasma rotation in the cusp derived from ϕ measurements. In the polar cap V_{56} assumed low, steadily eastward values. (6) Variations in the trace of B_{56} mimic those of quasi-dc values of $E_{X\text{-}Y}$ and E_Z. This indicates that Polar crossed several large-scale FAC sheets which close via Pedersen currents in the ionosphere [*Smiddy et al.*, 1980]. (7) Positive (negative) slopes in the B_{56} trace indicate FACs into (out of) the ionosphere. Consistent with a postnoon MLT trajectory, the positive (before 1505 UT) and negative (1505 - 1512 UT) slopes in B_{56} appear to be encounters with the afternoon Region 2 and Region 1 systems [*Iijima and Potemra*, 1976], respectively. The remaining FACs belong to the Region 0 system

[*Erlandson, et al.*, 1988]. As expected, the main Region 0 current has a polarity opposite to that of the adjacent Region 1. A small region of upward current is seen poleward of the main Region 0 current.

April 3, 1996

Plate 1B presents HYDRA measurements from 1200 to 1345 UT on April 3, 1996. Again, we divide the measurements as coming from four phenomenologically distinct regions. (1) Prior to ~1229 UT two populations of low- and high-energy electrons are sampled. From spectral similarities to fluxes detected at the same invariant latitudes during the previous pass, we identify them as photoelectrons and electrons from the CPS. Over the same period energetic (>1 keV) ion fluxes, whose mean energies decreased with increasing invariant latitude, were observed. (2) Fluxes of electrons with energies between about 500 eV and 4 keV underwent rapid increases and decreases at 1229 and 1238 UT, respectively. In this interval fluxes of ions with energies <200 eV rose above background. (3) From about 1238 to 1330 UT Polar crossed a region of high fluxes of electrons whose mean energies, except for a few small-scale structures, decreased smoothly with invariant latitude. This region is marked by two ion populations with energies centered near 500 eV and 7 keV. (4) After 1330 UT HYDRA detected polar rain electron and low ion flux levels, more typical of the polar cap. Again we describe particle from the first and fourth intervals as marking the CPS and polar cap, respectively. Sources for particles of the second and third will be discussed later.

Electric and magnetic field measurements from the same period are given in Figure 2. A magnetic field avoidance angle of 30° was used throughout for the electric field spin fits. Variations with time-scales of a few minutes or more in the spin-plane components of the electric field, $E_{X\text{-}Y}$ and E_Z track well with each other and with those of B_{56}, with the model field subtracted, over the entire interval. We see that large-amplitude fluctuations with periods near 10 s appear continuously between 1233 and 1300 UT, and in bursts near 1330 UT. The potential distribution detected by EFI, indicates that Polar was in a region of negative potential, characteristic of the afternoon convection cell. The plasma flow component $V_{56} = (E_{X\text{-}Y}\, B_Z - E_Z\, B_{X\text{-}Y})/B^2$ was weaker than observed on April 8, and after 1235 UT was predominantly toward the east. On large-scale, the trace of B_{56} appears similar to that observed on April 8. Positive slopes, indicating FACs into the ionosphere were observed before 1236 UT (region 2) and from 1248 to 1308 UT; a negative trend in the slope of B_{56} (Region 1)

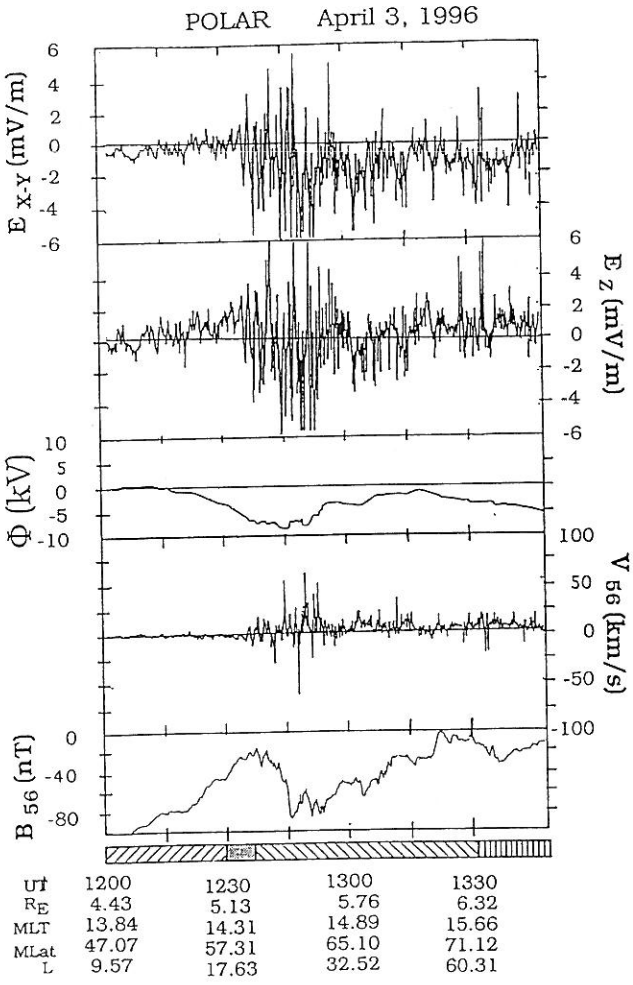

Figure 2. Electric and magnetic field measurements from 1200 – 1345 UT on April 3, 1996, in the same format as Figure 1.

appeared between these intervals. A significant difference between the B_{56} traces of Figures 1 and 2 is the abundance of low-frequency fluctuations with amplitudes of a few nT. Their correlation with electric field variations indicates that Polar encountered Alfvén waves in the Pc 4 and 5 bands, as well as the large-scale FAC systems and suggests a more dynamic environment than that of the April 8 pass. Finally we note that the sharp negative turns in the B_{56} trace at 1300 and 1304 UT coincide with small-scale bursts of electron found in Plate 1B.

DISCUSSION

Data from the two Polar passes with northward IMF exhibit both similarities and differences. The magnetic field variations are characteristic of the afternoon Regions 0, 1 and 2 systems of FACs. At the highest and lowest

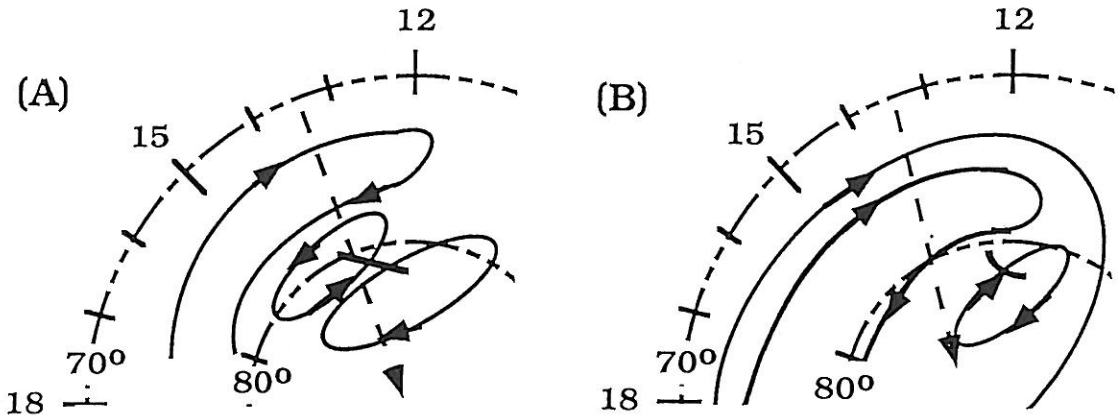

Figure 3. Schematic representation of ionospheric projection of potential distributions detected by Polar near (A) 1515 UT on April 8, 1996 and (B) 1300 UT on April 3, 1996. Directions of plasma flow are indicated by arrows.

invariant latitudes for which HYDRA spectral measurements are shown in Plates 1 and 2, one finds familiar characteristics of the CPS and polar cap. Localized bursts of kilovolt electrons are found in both instances near the poleward boundary of Region 2 currents. Since Region 2 currents are driven by pressure gradients in the plasma sheet [*Harel et al.*, 1981], and particle spectral characteristics do not point elsewhere, we suggest that the bursts originate in the outer CPS. Physical processes responsible for the observed flux increases must operate deeper in the magnetospheric than the Polar orbit. The most intriguing aspects of the two data sets were observed in the third particle segments (1505 – 1540 UT, April 8, and 1330 UT, April 3), which roughly spans the Regions 1 and 0 FACs. In both cases the segments of interest began as Polar entered the Region 1 current sheet and ended as it entered the polar cap. Between these boundaries significantly different observations were made. Our analysis and interpretation of the observations from this portion of the Polar orbits follows.

Figure 3a schematically represents the data constraints on the convection pattern encountered by Polar on April 8, projected onto the ionosphere. From 1505 to 1512 UT the plasma had an eastward drift component and the ion spectrogram displayed a "standard" dispersion signature. During periods of southward IMF, such ion-dispersion structures are normally regarded as time-of-flight effects as ions move from magnetic-merging sites on the magnetopause toward the ionosphere. With a northward IMF, the inner (low-latitude) portion of the LLBL is dominated by high-energy ions from the plasma sheet and the outer (high-latitude) portion by low-energy ions from the magnetosheath [*Eastman et al.*, 1976]. The apparent "standard" dispersion results from the superposition of these two populations. The separation of the two sources is even more evident in the second event (Plate 1B). During the period of the apparent "standard" dispersion, Polar moved about 1.1° in invariant latitude. This is the approximately the same latitudinal width of the LLBL observed above the *ionosphere* [*Smiddy et al.*, 1982]. An examination of the potential distribution measured between 1452 and 1512 UT, indicates that equipotentials in the CPS continue into the LLBL. Finally, our interpretation of the particles detected by HYDRA as coming from the LLBL is consistent with theoretical arguments developed by *Siscoe et al.* [1991] that the LLBL is the current generator for the dayside Region 1.

From 1512 to 1537 UT Polar crossed a positive potential cell in which plasma convection had an eastward (westward) drift component in its equatorward (poleward) parts. The "inverse" ion dispersion structure appeared in the poleward part. The simplest interpretation of these observations is that Polar went through the mid-altitude projection of the cusp. Magnetic merging with the northward IMF occurred at the cusp's poleward boundary. In this scenario, Polar crossed the magnetic mapping of the merging line (the heavy line in Figure 3a) where it encountered the highest energy ions of the "inverse" dispersion structure. After entering the polar cap, Polar again found itself in a region of negative potential. The question arises as to whether equipotentials with values >– 2 kV in the polar cap connect with those in the LLBL. The answer appears to be no. From the Polar trajectory in Figure 3a, it is clear that plasma drifting along such equipotentials would have to move with a west component. In fact, data in Figure 1 show that the plasma had an eastward drift component. For this reason we have represented the second negative potential cell as being made up of open flux circulating clockwise in the polar cap. HYDRA measurements of polar rain fluxes indicate

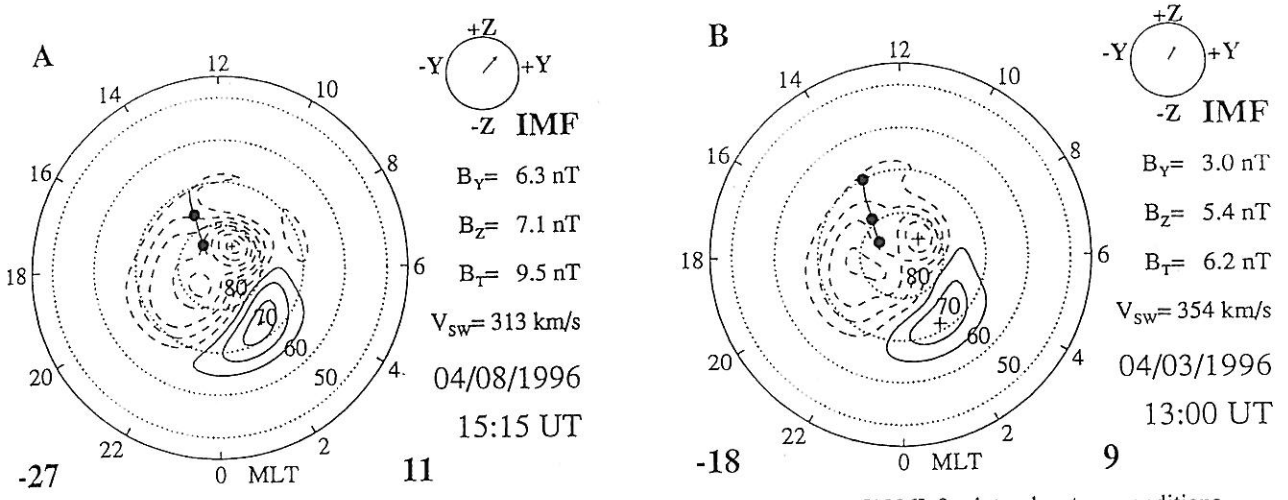

Figure 4. High-latitude potential distributions predicted by model of *Weimer* [1996] for interplanetary conditions prevailing near (A) 1515 UT on April 8, 1996, and (B) 1300 UT on April 3, 1996. The IMF values are averages over 40 minutes prior to the stated time of the data projected to the magnetopause in accordance with the measured solar wind velocity. The projected Polar orbit tracks using the *Tsyganenko* [1996] T-96 model are shown. The dots represent satellite projected positions at 1500 and 1600 UT on April 8, 1996 (A) and at 1200, 1300 and 1400 UT on April 3, 1996 (B).

that the satellite must have passed to the poleward side of this cell's merging line.

Figure 3b provides a sketch of the data constraints on the convection directions in the pattern crossed by Polar on April 3, based on the potential distribution found in the third panel of Figure 2. There are two classes of equipotentials with westward drifting plasma in the region of CPS fluxes. Equipotentials crossed at the lowest latitudes are not intersected again by the orbit. At higher latitudes within the CPS, we find equipotentials that turn and are intersected for a second time between 1240 and 1330 UT as the potential increased from about -8 to -1.5 kV. It encompasses the Region 1 and Region 0 current systems and spans the invariant-latitude range 76.5° to 82.6°. Ion fluxes observed across the entire interval are generally weak with broad distributions in energy. In the equatorwardmost portion (1240 – 1255 UT) they appear bimodal in energy indicating that they are of LLBL origin [*Eastman et al.*, 1976].

Electric potential and particle measurements are most simply explained if Polar remained within a projection of the boundary layer until it entered the polar cap. First, the electron fluxes observed in the early part of the boundary layer are higher in energy than those observed in the cusp on April 8, consistent with the findings of *Newell et al.* [1991b]. Second, the observed ion fluxes are an order of magnitude less than those observed in the cusp on April 8 and are more characteristic of boundary layer fluxes [*Haerendel et al.*, 1978]. Third, throughout the 1255 – 1330 UT period EFI measurements indicate that the plasma drift had an eastward component. During periods of IMF $B_Y > 0$, independent of the sign of IMF B_Z, magnetic tension forces on newly opened flux causes plasma to drift toward noon (west of the Polar orbit) then into the morning side of the polar cap. This is opposite to the observed eastward direction. Indeed the *Tsyganenko* [1996] model predicts that field lines near 80) and 1500 MLT map to the night rather than to the dayside of the magnetosphere. The observed fluxes must be coming from boundary layers somewhere back in the tail. Fourth, electron and ion fluxes observed between 1255 and 1330 UT show gradual, rather than abrupt, transitions to polar cap levels. This is seen most clearly in the electrons, whose average energies monotonically decreased with increasing invariant latitude. It may be viewed as due to an adiabatic cooling of electrons as flux tubes grow in volume and convect down stream along the flank of the magnetotail. The latitudinal width of the projection of this boundary layer is larger than that reported by *Smiddy et al.* [1982]. We note, however, that potential drop of ~8 kV measured across the boundary layer is similar to potentials reported by *Smiddy et al.* [1982] and in ISEE 1 observations of potentials across the low latitude boundary layer on the dusk side [*Mozer,* 1984]. Independent evidence of the boundary layer hypothesis is provided by the TIMAS ion mass spectrometer on Polar [*Shelley et al.*, 1995] which detected weak, variable low-energy fluxes of He^{++} during the interval which must have entered the boundary layer some distance down the tail.

Figures 4a and 4b present ionospheric potential distri-

butions in ILT/MLT predicted by the model of *Weimer*, [1995, 1996] for interplanetary conditions prevailing during the periods of interest on April 8 and April 3, respectively. Below the circular grids are listed minimum and maximum potentials predicted for the afternoon and morning cells; –28 and +12 kV on April 8, –18 and +9 kV on April 3. Polar trajectories, mapped to the ionosphere using the T-96 magnetic field model [*Tsyganenko*, 1996], are provided for reference. In both cases the model correctly predicts that Polar should detect measurable convection poleward of 72° ILT, and that over the studied periods, it should remain within the afternoon cell. The morning (positive potential) cell is restricted to the postmidnight – predawn quadrant. In both cases the model predicts that small lobe cells should develop in the noon sector, poleward of 80° ILT. The sense of rotation for convection in these cells is clockwise, similar to that reported by *Burke et al.*, [1994] for northward IMF with $By > 0$. Attention is directed to the fact that even though IMF clock angles for the two events are similar, their differences, along with dipole tilt angle distinctions, are sufficient to produce clear differences in predicted convection patterns for the early afternoon sector. The model correctly predicted that Polar would pass through a more stagnant region near 80° ILT on April 3 than on April 8.

A comparison of the potential distributions shown in Figures 3 and 4 also reveals some significant differences. Obviously the model did not predict Polar's encounter with a positive potential cell during the April 8, pass. The data are more suggestive of a four-cell pattern [*Burke et al.*, 1979; *Reiff and Heelis* 1994] than a distorted two-cell pattern with an embedded lobe cell [*Burke et al.*, 1994]. *Rich and Hairston* [1994], suggested that the four-cell pattern may occur so rarely that it is not reproduced by empirical models developed from large data bases. However, the model of *Weimer* [1995, 1996] does produce the positive potential lobe cell on the dusk side of noon for pure northward IMF in a structured four-cell configuration, and this may be the start of the development of that cell.

Acknowledgments. This work was performed under funding from the NASA GGS Program (part of the International Solar Terrestrial Physics Program). Work at UC Berkeley and Mission Research Corporation was supported under contract number NAS5-30367 and grant number NAG5-3182. Work at UCLA was supported under grant number NAG5-3171. Work at Iowa was supported under grant NAG S-2231. WKP was supported by contract NAS5-33032. WJB was supported in part by NASA and in part by the U. S. Air Force Office of Scientific Research task 2311PL014. We thank R. Lepping and K. W. Ogilvie for the use of the WIND magnetic field and plasma data.

REFERENCES

Basinska, E. M., W. J. Burke, N. C. Maynard, W. J. Hughes, J. D. Winningham, and W. B. Hanson, Small-scale electrodynamics of the cusp with northward interplanetary magnetic field, *J. Geophys. Res.*, *97*, 6369, 1992.

Burch, J. L., P .H. Reiff, R. A. Heelis, R. W. Spiro, and S. A. Fields, Cusp region particle precipitation and ion convection for northward interplanetary field, *Geophys. Res. Lett.*, *7*, 393, 1980.

Burke, W. J., E. M. Basinska, N. C. Maynard, W. B. Hanson, J. P. Slaven, and J. D. Winningham, Polar cap potential distributions during periods of positive IMF By and Bz, *J. Atmos. Terres. Phys.*, *56*, 209, 1994.

Burke, W. J., M. C. Kelley, R. C. Sagalyn, M. Smiddy, and S. T. Lai, Polar cap electric field structures with northward interplanetary magnetic field, *Geophys. Res. Lett.*, *6*, 21, 1979.

Clauer, C. R., and E. Friis-Christensen, High-latitude electric fields and currents during strongly northward magnetic field: observations and model simulations, *J. Geophys. Res.*, *91*, 6959, 1986.

Doering, J. P., W. K. Peterson, C. O. Bostrom and T. A. Potemra, High resolution daytime photoelectron energy spectra from AE-E, *Geophys. Res. Lett.*, *3*, 129, 1976.

Dungey, J. W., Interplanetary magnetic field and the auroral zones, *Phys. Rev. Lett.*, *6*, 47, 1961.

Erlandson, R. E., L. J. Zanetti, T. A. Potemra, P. F. Bythrow, and R. Lundin, IMF By dependence of region 1 Birkeland currents near noon, *J. Geophys. Res.*, *93*, 9804, 1988.

Eastman T. E., E. W. Hones Jr., S. J. Bame, and J. R. Asbridge, The magnetospheric boundary layer: site of plasma, momentum and energy transfer from the magnetosheath into the magnetosphere, *Geophys. Res. Lett.*, *3*, 685, 1976.

Haerendel, G., G. Paschmann, N. Sckopke, H. Rosenbauer, and P. C. Hedgecock, The frontside boundary layer of the magnetosphere and the problem of reconnection, *J. Geophys. Res.*, *83*, 3195, 1978.

Hanson, W. B., R. A Heelis, R. A. Power, C. R. Lippincott, D. R. Zuccaro, B. J. Holt, L. H. Harmon, and S. Sanatani, The retarding potential analyzer for Dynamics Explorer-B, *Space Sci. Instru.*, *5*, 503, 1981.

Harel, M., R. A. Wolf, P. H. Reiff, R. W. Spiro, W. J. Burke, F. J. Rich, and M. Smiddy, Quantitative simulation of a magnetospheric substorm 1. Model logic and overview, *J. Geophys. Res.*, *86*, 2217, 1981.

Harvey, P., et al., The electric field instrument on the Polar satellite, in *The Global Geospace Mission*, ed. by C. T. Russell, p. 583, Kluwer Academic Publishers, Dordrecht, The Netherlands, 1995.

Heppner J.P., and N.C. Maynard, Empirical high-latitude electric field models, *J. Geophys. Res.*, *92*, 4467, 1987.

Iijima, T., and T. A. Potemra, Field aligned currents in the dayside cusp observed by TRIAD, *J. Geophys. Res.*, *81*, 5971, 1976.

Iijima, T., and T. Shibaji, Global characteristics of northward IMF-associated (NBZ) field-aligned currents, *J. Geophys. Res.*, *89*, 2408, 1984.

Maezawa, K., Magnetospheric convection induced by positive and negative Z components of the interplanetary magnetic field: Quantitative analysis using polar cap magnetic records, *J. Geophys. Res.*, *81*, 2289, 1976.

Maynard, N. C., Structure in the dc and ac electric fields associated with the dayside cusp region, in *The Polar Cusp*, edited by J.A. Holtet and A. Egeland, p. 305, D. Reidel, Hingham, MA, 1985.

Maynard, N. C., T. L. Aggson, E. M. Basinska, W. J. Burke, P. Craven, W. K. Peterson, M. Sugiura and D. R. Weimer, Magnetospheric boundary dynamics: De-1 and DE-2 observations near the magnetopause and cusp, *J. Geophys. Res.*, *96*, 3505, 1991.

Mozer, F. S., Electric field evidence on the viscous interaction at the magnetopause, *Geophys. Res. Lett*, *11*, 135, 1984.

Murphree, J. S., R. D. Elphinstone, D. Hearn and L. L. Cogger, Large-scale high-latitude dayside auroral emissions, *J. Geophys. Res.*, *95*, 2345, 1990.

Newell, P. T., W. J. Burke, C. -I. Meng, E. R. Sanchez, and M. E. Greenspan, Identification and observation of plasma mantle flow at low altitude, *J. Geophys. Res.*, *96*, 21,013, 1991a.

Newell, P. T., W. J. Burke, E. R. Sanchez, C. -I. Meng, M. E. Greenspan, and C. R. Clauer, The low-latitude boundary layer and the boundary plasma sheet at low altitude: prenoon precipitation regions and convection reversal boundaries, *J. Geophys. Res.*, *96*, 35, 1991b.

Reiff, P. H. and R. A. Heelis, Four cells or two? Are four cells really necessary?, *J. Geophys. Res.*, *99*, 3955, 1994.

Reiff, P. H., and J.L. Burch, IMF *By*-dependent plasma flow and Birkeland currents in the dayside magnetosphere, 2. A global model for northward and southward IMF, *J. Geophys. Res.*, *90* 1595, 1985.

Reiff, P. H., J. L. Burch, and R. W. Spiro, Cusp proton signatures and the interplanetary magnetic field, *J. Geophys. Res.*, *85*, 5997, 1980.

Rich, F. J., and M. Hairston, Large-scale convection patterns observed by DMSP, *J. Geophys. Res.*, *99*, 3827, 1994.

Russell, C. T., The configuration of the magnetosphere, *in Critical Problems of Magnetospheric Physics*, edited by E. R. Dryer, p. 1, IUCSTP, National Academy of Sciences, Washington, DC, 1972.

Russell, C. T., R. C. Snare, J. D. Means, D. Pierce, D. Dearborn, M. Larson, G. Barr, and G. Le, The GGS/Polar magnetic field investigation, in *The Global Geospace Mission*, edited. by C. T. Russell, p. 563, Kluwer Academic Publishers, Dordrecht, The Netherlands, 1995.

Sandholt, P. E., Auroral electrodynamics at the cusp/cleft poleward boundary during northward interplanetary magnetic field, *Geophys. Res. Lett*, *18*, 805, 1991.

Sandholt, P. E., C. J. Faruggia, M. Øieroset, P. Staunning, and S. W. H. Cowley, Auroral signature of lobe reconnection, *Geophys. Res. Lett*, *23*, 1725, 1996.

Scudder, et al., HYDRA – a 3 dimensional electron and ion hot plasma instrument for the Polar spacecraft of the GGS mission, in *The Global Geospace Mission*, edited by C. T. Russell, p. 459, Kluwer Academic Publishers, Dordrecht, The Netherlands, 1995.

Shelley, et al., The toroidal imaging ion mass spectrograph (TIMAS) for the Polar mission, in *The Global Geospace Mission*, edited by C. T. Russell, p. 497, Kluwer Academic Publishers, Dordrecht, The Netherlands,1995.

Siscoe, G. L., W. Lotko, P. H. Reiff, and B. U. Ö. Sonnerup, A high-latitude, low-latitude boundary layer model of the convection current system, *J. Geophys. Res.*, *96*, 3487, 1991.

Smiddy, M., W. J. Burke, M. C. Kelley, N. A. Saflekos, M. S. Gussenhoven, D. A. Hardy, and F. J. Rich, Effects of high-latitude conductivity on observed convection electric fields and Birkeland currents, *J. Geophys. Res.*, *85*, 6811, 1980.

Tsyganenko, N. A., Effects of the solar wind conditions on the global magnetospheric configuration as deduced from data based field models, *Third International Conference on Substorms (ICS-3), ESA SP-389*, p. 181, ESA Pub. Div., Noordwijk, The Netherlands, 1996.

Weimer, D. R., A flexible, IMF dependent model of high latitude electric potentials having "space weather" applications, *Geophys. Res. Lett.*, *23*, 2549, 1996.

Weimer, D. R., Models of high-latitude electric potentials derived with a least square error fit of spherical harmonic coefficients, *J. Geophys. Res.*, *100*, 19,595, 1995.

Winningham, J. D., J. L. Burch, N. Baker, V. A. Blevins and R. A. Hoffman, The low altitude plasma instrument (LAPI), *Space Sci. Instru.*, *5*, 465, 1981.

W. J. Burke, Phillips Laboratory, 29 Randolph Road, Hanscom AFB, MA 01731. (email: burke@plh.af.mil)

N. C. Maynard and D. R. Weimer. Mission Research Corporation, One Tara Blvd., Suite 302, Nashua, NH 03062. (email: nmaynard@mrcnh.com; dweimer@mrcnh.com)

F. S. Mozer, Space Science Laboratory, Grizzly Peak Drive, University of California, Berkeley, CA 94720. (email: fmozer@sunspot.ssl.berkeley.edu)

W. K. Peterson, Lockheed Martin Palo Alto Research Laboratory, 3251 Hanover St., Palo Alto, CA 94304. (email: pete@space.lockheed.com)

C. T. Russell, Institute for Geophysics and Planetary Physics, University of California at Los Angeles, Los Angeles, CA 90049. (email: ctrussell@igpp.ucla.edu)

J. D. Scudder, Department of Space Physics and Astronomy University of Iowa, Iowa City, IA, 52240. (email: jds@space-theory.physics.uiowa.edu)